13th ewtec 2019 Proceedings of the 13th European Wave and Tidal Energy Conference 1-6 Sept 2019, Naples, Italy

Numerical investigation on the effects of the pitch angle on the efficiency of an Archimedean-type turbine

Gianluca Zitti, Fernando Fattore, Alessandro Brunori, Bruno Brunori and Maurizio Brocchini

***Abstract*—We study an innovative turbine, the Archimedean-Type Hydrokinetic Turbine, for the renewable energy extraction from tidal stream. It is similar to the well-known Archimedean Screw, used in several small hydropower plants, but is used here in hydrokinetic mode: all the devices for water canalization are absent and the turbine is placed in a stream. Using this setup the operating principle totally changes: the classical Archimedean Screw exploits the difference in potential energy between two water reservoirs, while the Archimedean-Type Hydrokinetic Turbine exploits the kinetic energy of a flow and can be placed, for example, in a tidal current. The combination of the operational requirements (i.e. installation and energy transfer) and of the current variability can change in time the incidence angle, i.e. angle between the flow direction and the turbine axis. Numerical experiments are here used to investigate the role of the incidence angle on the performance of the turbine. The hydrodynamics are simulated using a three-dimensional numerical model that implements the RANS equations for incompressible water, closed with an SST $k-\omega$ turbulence model. In particular, the efficiency for different incidence angles and different tip speed ratios is evaluated using Betz theory, which is commonly used for the evaluation of the efficiency of complex geometry hydrokinetic turbines. Efficiency curves for different incidence angles are derived and compared, to quantify the influence on the power production and on the efficiency of the turbine.**

***Index Terms*—Renewable energy, Tidal Stream, Hydrokinetic Turbine, Archimedes Turbine, Efficiency Evaluation.**

I. Introduction

TIDAL energy is a possible (and innovative) answer to the demand of renewable energies for a sustainable development, which is one of the main issues of our era [1]. Many tidal energy technologies are in development stages and some of them already exploit the tidal currents forced through natural or artificial constrictions, by means of hydrokinetik turbines [2]. Hydrokinetic turbines may have different shapes, but they are all based on the design of hydrofoils, optimized to create the maximum lift and minimum drag [2]–[5]. Among the hydrokinetic turbine, used in river flow, we can find the Archimedes turbine, which has been used since the ancient age to extract energy from river flows, exploiting a water head jump, i.e. the potential energy, of the water. However, the shape of the Archimedes turbine (a screw where the blades are continuously attached to the turbine axis) suggested to use it as an hydrokinetic turbine, as proved by the preliminary results in [6], [7].

The development of an Archimedean-Type Hydrokinetic Turbine came from an idea of Soc. Neferti Srl, which designed and realized several prototypes of this kind of Archimedean-Type Hydrokinetic Turbine. Field tests showed interesting responses and suggested a rigorous study of the turbine by means of numerical simulations. The study, carried out by the Hydraulic research group of the Polytechnic University of Marche, focussed on the evaluation of the performance of the machine and on optimizing the fundamental design parameters. The idea of an effective Archimedean-Type Hydrokinetic Turbine aimed at producing a device that: 1) is simple and cheap, therefore it can be used in location with limitation, such as in shipping areas, 2) reduces environmental impacts, 3) does not require the construction of civil infrastructures (barrages, reservoirs), 4) works also in small water depths and 5) maximizes the flow energy exploitation.

Since geometrical limitation of the location can be of large importance in tidal stream energy exploitation [2], the shape of the turbine can have an important role in the management of the spaces: in this context, the screw turbines are different to other hydrokinetc turbines with horizontal axis: their dimension can be increased both axially and radially and they can be inclined of $10°$ with respect to the stream direction, without losing power production [6], [7]. However, the role of the inclination of the turbine axis with respect to the stream direstion requires a more detailed analysis. For this reason, in this work we report some preliminary numerical results on the effect of the incidence angle on the performance of the Archimedean-Type Hydrokinetic Turbine. The power production P_t and the performance coefficient C_p of an Archimedean-Type Hydrokinetic Turbine is investigated by means of numerical simulations, run by varying the incidence angle. Section II illustrates the theoretical model used to evaluate the performance, section III reports the numerical implementation of the model, while results are reported in section IV. Finally, section V discusses the performance of the Archimedean-Type Hydrokinetic Turbine in relation to the incidence angle and closes the paper.

Paper ID number: 1733. Conference Track:TDD

G. Zitti and M Brocchini are with Departement of Construction, Civil Engineering and Architecture, Polytechnic University of Marche, Ancona, Italy (e-mail: g.zitti@univpm.it ; m.brocchini@univpm.it).

F. Fattore was consultant for Neferti S.r.L. Milano, Milano, Italy (e-mail :ferfat@libero.it).

A Brunori and B. Brunori are with Neferti S.r.L. Milano, Milano, Italy (e-mail :abrunori@neferti.it ; octave@neferti.it).

II. Theoretical basis

Hydrokinetic turbine theory is derived from wind turbines theory, such as several types of tidal stream turbines have been borrowed from the wind industry (e.g. the horizontal axis rotor turbines [8], [9] and the Savonius turbines [10]–[14]). Following the wind and hydrokinetic turbine theory [15], the efficiency of the turbine is measured using the performance coefficient C_p:

$$C_p = P_t/P_f \tag{1}$$

where P_t is the power generated by the screw turbine and P_f is the power available from the fluid flow. The power generated by the screw turbine can be evaluated as

$$P_t = M_t\omega \tag{2}$$

where M_t is the torque generated by the fluid on the turbine (that can be transferred to an electric generator) and ω is the turbine rotation velocity. From Betz theory, the power available from the fluid flow is:

$$P_f = \frac{1}{2}\rho A v^3 \tag{3}$$

where ρ and v are the fluid density and stream flow velocity, respectively, while A is the cross-section area. Betz theory is based on a simplified geometrical model, where the turbine is assumed a 2D circular rotor, crossed by a perpendicular flow. Thus, in the Betz theory the cross sectional area is simply evaluated as the area of a circle with the same radius R of the turbine:

$$A_B = R^2\pi \tag{4}$$

This value can be evaluated also for the screw turbine, but if we consider an inclined configuration of a screw turbine, the actual projection of the surface that fronts the flow on a plane perpendicular to the flow is not a simple circle. Representing the Archimedean-Type Hydrokinetic Turbine with a circular cylinder that envelops the turbine (see Fig. 1), the area A depends on the angle θ between the turbine axis and the stream flow direction (i.e. the incidence angle) as given by the following geometrical relation:

$$A_S = R^2\pi\cos(\theta) + 2RLsin(\theta) \tag{5}$$

where R and L are the cylinder radius and length, respectively. It is evident that the inclination of the

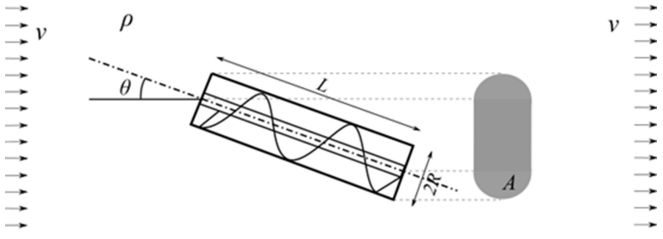

Fig. 1. Sketch of the physical model. The projection of the surface that fronts the flow is reported in grey.

turbine axis with the flow could have an important influence for an Archimedean-Type Hydrokinetic Turbine: by increasing the cross sectional area (5), the available power (3) increases. Therefore, an increase in available power can result in an increase in extracted power but, since it appears at the denominator in (1), it can also result in an efficiency decrease. In the following, the performance coefficient C_p has been evaluated with both formulations of the cross section area, respectively being representative of the dependence on the incidence angle of the generated power the first (4) and of the actual efficiency the second (5). For hydrokinetic turbines, the performance coefficient C_p is conventionally represented as function of the Tip Speed Ratio (TSR):

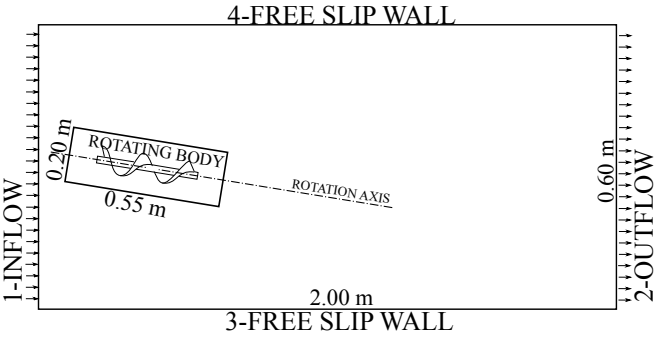

Fig. 2. Sketch of the numerical model, with generic incidence angle.

$$TSR = \frac{\omega R}{v} \tag{6}$$

If the geometry of the turbine is assigned, the performance coefficient only depends on the Tip Speed Ratio and on the incidence angle: $C_p = C_p\,(TSR, \theta)$. Therefore, in the following sections, the geometry of an Archimedean-Type Hydrokinetic Turbine has been fixed and its performance studied by varying the TSR (as commonly done for other hydrokinetic turbines) and the incidence angle θ.

III. Numerical model

To evaluate the performances of the Archimedean-Type Hydrokinetic Turbine, numerical simulations have been performed with the commercial software Academic Ansys Fluent.

The physical model was composed by an Archimedes screw turbine immersed in a water flume (see Fig. 2) where a flow was imposed, using inflow-outflow boundary conditions, assigning the velocity $v = 0,2$ m/s at opposite upstream/downstream boundaries. Free slip wall boundary conditions were assigned at the other four boundaries.

The screw model was composed by an axle with diameter 20 m^{-3} and a two stride blade 5 m^{-3} thick, with external radius $R = 50$ m^{-3}. Each stride was long $p = 160$ m^{-3}. The blade was not perpendicular to the axle, but inclined of $70°$. The fluid volume was a parallelepiped 2 m long in the streamwise direction, 1 m wide and 0.6 m high. The inclination of the turbine has been varied from $\theta = 0°$ to $\theta = 60°$, with steps of $10°$. A configuration with generical angle was shown in Fig. 2. In all configurations the turbine axle midpoint was located at the center of the crossflow section, at a

TABLE I
MESH SIZE FOR EACH GEOMETRICAL CONFIGURATION

Incidence angle θ [°]	Number of cells	Number of nodes
0	529599	157111
10	527710	141946
20	505573	152997
30	505627	153035
40	511859	154109
50	511370	154009
60	506200	153124

distance of 0.4 m from the inflow boundary. The incidence angle was varied rotating the turbine around this fixed point. In this manner, the distance of the turbine was always at least $4R$ from the inflow boundary and at least $30R$ from the outflow boundary, minimizing boundary effects [8].

The multiple reference frame method was used [16] to solve the transient hydrodynamics due to the flow and to the turbine rotation. The domain was divided into two parts: 1) a rotating body, which is a cylindrical volume with radius twice the turbine diameter and length 0.55 m, which contained the turbine and 2) the complementary to the parallelepiped fluid domain (see Fig. 2).

The mesh was generated separately in the two parts and the rotating body was rotated at each time step with an assigned angular velocity ω. The solutions of the two domains were calculated in the different reference frames for each part and the boundary conditions for the inner rotating body were evaluated by interpolation on the contact surface. In the reference frame of the rotating body the turbine is steady, but in the fixed reference frame it rotates with the assigned water speed. In that sense the simulation is transient. The domains were discretized in linear tetrahedral cells, with maximum size of $3 \cdot 10^{-2}$ m, with mesh refinement on the surface of the screw, where the mesh size was $3 \cdot 10^{-3}$ m. Perpendicular to the turbine wall an inflation of twelve layers was assigned, with first layer thickness equal to $1 \cdot 10^{-4}$ m and growth rate of 1.4. A representation of the refinement is reported in Fig. 3. The sensivity of the results to the boundary layer meshing was analysed in [7], where the results of simulations with a refined mesh in the boundary layer was found to lie in a small range around the reported simulation.

The geometry of the domain and the generated mesh varied with the incidence angle θ. The mesh size was similar in all configurations and the specific values of cells and nodes are reported in Table I.

The solution was calculated with a pressure-based model, which solved the discretized form of the Reynolds Averaged Navier Stokes Equation. The turbulence model used to close the equations was the Menter's $k-\omega$ Shear Stress Transport ($k-\omega$ SST) model, which works well with adverse pressure gradients and separating flow [17]–[19]. For each configuration, the angular velocity of the turbine was varied from $\omega = 1$ rad/s to $\omega = 6$ rad/s with steps of 0.5 rad/s,

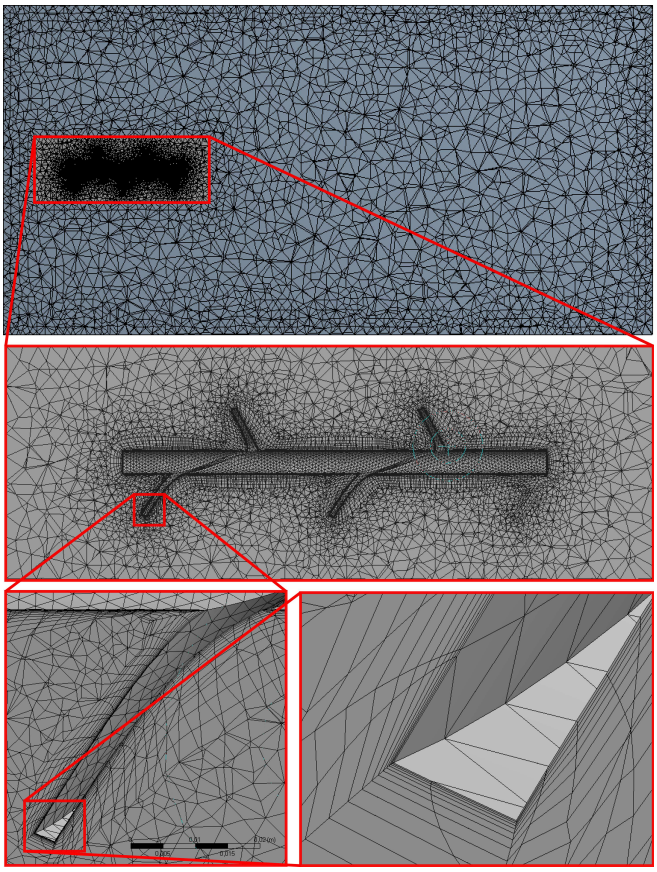

Fig. 3. Sample of the mesh generated on a longitudinal plane (top panel) and zoom of the mesh refinement in the proximity of the turbine (middle panel) and of the inflation along the turbine surface (bottom panels).

thus varying the TSR from 0.25 to 1.5, with steps of 0.125. For each configuration and flow condition, a simulation was run for a duration of at least 10 s. For the slower speed ($\omega = 1$ rad/s) two rotation were reproduced, while 10 rotations were reproduced for the faster speed ($\omega = 6$ rad/s). The time step is fixed to 0.2 s for all simulations. This reduces the resolution of the description of the rotation as the rotation speed increases, but it does not affect the final time-averaged results. Convergence iterations at each time step were run up to a relative error of 10^{-3} for mass conservation and 10^{-4} for the velocities, with a maximum number of 50 iterations for each time step.

Results of the numerical experiments are reported in the subsequent section.

IV. RESULTS

For each numerical simulaton described in the previous section, the torque M_t was calculated as the time-averaged value of the torque resultant from pressures and shear stresses of the fluid on the turbine surface. For this calculation, the initial stage peak (i.e. the transient phase, evident in the torque evolution, with a duration between 3 and 5 s) was neglected. The torque M_t was used in (2) to evaluate the extracted power P_t and the performace coefficient in (1).

As said before, two expressions of the cross sectional area have been used to evaluate the flow power: the

TABLE II
CROSS-SECTION AREA A_S AND AVAILABLE POWER P_{fS}, VARYING WITH THE INCIDENCE ANGLE θ

θ	A_S [m]	P_{fS} [mW]
0	0.0079	31.4159
10	0.0133	53.1656
20	0.0183	73.2999
30	0.0228	91.2070
40	0.0266	106.3428
50	0.0296	118.2475
60	0.0316	126.5592

Betz formula $P_{fB} = 0.5\rho A_B v^3$, using (4) for the cross-section area, and the formula adapted to the inclined screw $P_{fS} = 0.5\rho A_S v^3$, using (5) for the cross-section area. The values of A_S and P_{fS}, varying with θ are reported in Table II; the values of A_B and P_{fB} correspond to the values of A_S and P_{fS} for $\theta = 0$.
The two different values of the flow available power were used in (1) to evaluate two different expression of the performance coefficient: $C_{pB} = P_t/P_{fB}$, which is more representative of the dependence of the generated power on the incidence angle, and $C_{pS} = P_t/P_{fS}$, which is more representative of the efficiency. These efficiency results are reported in Table III

V. DISCUSSION AND CONCLUSIONS

The performance of an Archimedean-Type Hydrokinetic Turbine have been evaluated through dedicated numerical experiments, focussed on the dependence of the machine power production and efficiency on the incidence angle.

A. Dependence of the power production on the incidence angle

The dependence of the power production on the incidence angle is described by the performance coefficient: C_{pB}, reported in Fig. 4 in relation to the TSR, for different incidence angles. We first notice that all the power production range was investigated for each incidence angle and every efficiency curve has the typical bell shape of the performance curves of other hydrokinetic turbines (e.g. [20], [21]). The best power production varies with the incidence angle θ: for $\theta = 0°$ the best power production is $C_{pB} = 23.8\%$ and occurs for $TSR = 0.75$. Increasing the incidence angle the best power production increases up to reach the maximum value of $C_{pB} = 31.3\%$, which occurs for $\theta = 40°$ and $TSR = 1$. For incidence angles greater than $40°$ the power production decreases: in fact for $\theta = 60°$ the maximum performance is $C_{pB} = 23.3\%$ and occurs for $TSR = 0.75$. In summary, the power production has a maximum for $\theta \sim 40°$ and this increase in power production corresponds to an increase also in TSR.

In addition, increasing the incidence angle, the performance curves show a deviation from the typical bell shape. Moving from $\theta = 0°$ to $\theta = 60°$ the bell loses symmetry, the maximum moves to the right and the increasing branch of the curve is less steep than the increasing branch.

TABLE III
RESULTS

ID (θ , TSR)	P_t [mW]	C_{pB}	C_{pS}
0 , 0.250	4.461	14.2%	14.2%
0 , 0.375	5.587	17.8%	17.8%
0 , 0.500	6.418	20.4%	20.4%
0 , 0.625	7.256	23.1%	23.1%
0 , 0.750	7.468	23.8%	23.8%
0 , 0.875	7.242	23.1%	23.1%
0 , 1.000	6.756	21.5%	21.5%
0 , 1.125	5.891	18.8%	18.8%
0 , 1.250	4.825	15.4%	15.4%
0 , 1.375	3.425	10.9%	10.9%
0 , 1.500	1.765	5.6%	5.6%
10 , 0.250	4.456	14.2%	8.4%
10 , 0.375	5.924	18.9%	11.1%
10 , 0.500	6.869	21.9%	12.9%
10 , 0.625	7.384	23.5%	13.9%
10 , 0.750	7.631	24.3%	14.4%
10 , 0.875	7.668	24.4%	14.4%
10 , 1.000	7.390	23.5%	13.9%
10 , 1.125	6.724	21.4%	12.6%
10 , 1.250	5.657	18.0%	10.6%
10 , 1.375	4.289	13.7%	8.1%
10 , 1.500	2.623	8.3%	4.9%
20 , 0.250	4.439	14.1%	6.1%
20 , 0.375	6.326	20.1%	8.6%
20 , 0.500	7.623	24.3%	10.4%
20 , 0.625	8.653	27.5%	11.8%
20 , 0.750	9.212	29.3%	12.6%
20 , 0.875	9.248	29.4%	12.6%
20 , 1.000	8.918	28.4%	12.2%
20 , 1.125	8.252	26.3%	11.3%
20 , 1.250	7.250	23.1%	9.9%
20 , 1.375	5.817	18.5%	7.9%
20 , 1.500	3.955	12.6%	5.4%
30 , 0.250	4.717	15.0%	5.2%
30 , 0.375	6.596	21.0%	7.2%
30 , 0.500	7.872	25.1%	8.6%
30 , 0.625	8.827	28.1%	9.7%
30 , 0.750	9.434	30.0%	10.3%
30 , 0.875	9.712	30.9%	10.6%
30 , 1.000	9.657	30.7%	10.6%
30 , 1.125	9.199	29.3%	10.1%
30 , 1.250	8.146	25.9%	8.9%
30 , 1.375	6.367	20.3%	7.0%
30 , 1.500	3.970	12.6%	4.4%
40 , 0.250	4.417	14.1%	4.2%
40 , 0.375	6.026	19.2%	5.7%
40 , 0.500	7.396	23.5%	7.0%
40 , 0.625	8.388	26.7%	7.9%
40 , 0.750	9.226	29.4%	8.7%
40 , 0.875	9.748	31.0%	9.2%
40 , 1.000	9.827	31.3%	9.2%
40 , 1.125	9.057	28.8%	8.5%
40 , 1.250	7.412	23.6%	7.0%
40 , 1.375	4.952	15.8%	4.7%
40 , 1.500	1.762	5.6%	1.7%
50 , 0.250	3.784	12.0%	3.2%
50 , 0.375	5.313	16.9%	4.5%
50 , 0.500	6.435	20.5%	5.4%
50 , 0.625	7.652	24.4%	6.5%
50 , 0.750	8.615	27.4%	7.3%
50 , 0.875	9.189	29.2%	7.8%
50 , 1.000	8.680	27.6%	7.3%
50 , 1.125	6.971	22.2%	5.9%
50 , 1.250	4.394	14.0%	3.7%
60 , 0.250	3.225	10.3%	2.5%
60 , 0.375	4.391	14.0%	3.5%
60 , 0.500	5.305	16.9%	4.2%
60 , 0.625	6.244	19.9%	4.9%
60 , 0.750	7.332	23.3%	5.8%
60 , 0.875	6.710	21.4%	5.3%
60 , 1.000	5.020	16.0%	4.0%
60 , 1.125	2.360	7.5%	1.9%

Some results are not reported (i.e. $\omega \geq 5.5$ rad/s for $\theta \geq 50°$), since they provided negative torque.

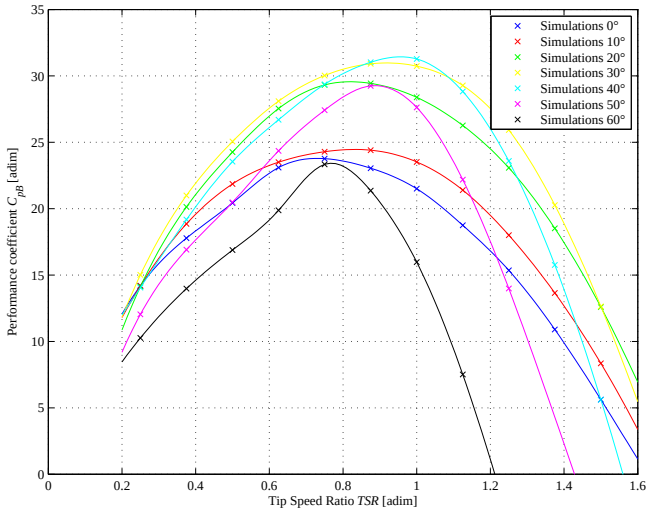

Fig. 4. Performance coefficient C_{pB}, evaluated with the fixed cross-section area $A_S = \pi R^2$. Crosses corresponds to numerical results, lines are spline interpolation.

B. Dependence of the efficiency on the incidence angle

The dependence of the efficiency on the incidence angle is described by the performance coefficient: C_{pS}, reported in Fig. 5 in relation to the TSR, for different incidence angles. We find, again, the bell shape of the

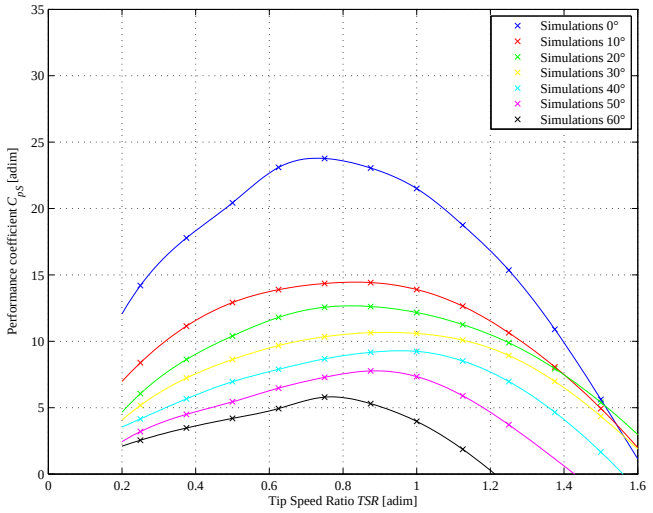

Fig. 5. Performance coefficient C_{pS}, evaluated with the screw-adapted cross-section area $R^2\pi\cos(\theta) + 2RLsin(\theta)$. Crosses correspond to numerical results, lines are spline interpolation.

performance curves, but the role of the incidence angle θ is more significant here. The available power P_{fS} (evaluated with the cross-section area A_S) significantly reduces the performance in (5) for $\theta \geq 0°$ and the efficiency decreases monotonically with the increase of the incidence angle θ. The best performance for $\theta = 0°$ is $C_{pS} = 23.3\%$. It drops to $C_{pS} = 14.4\%$ for $\theta = 10°$ and keeps decreasing down to $C_{pS} = 5.8\%$ for $\theta = 60°$. In summary, the best performance C_{pS} is obtained when the axis of the turbine is aligned with the stream flow (see Fig. 5), but the power provided C_{pB} in inclined configurations with incidence angle lower than $50°$ is larger than that provided in aligned configuration (see Fig. 4). This suggests that the lower performances in the inclined configurations are mainly due to the increase of the cross section area A_S.

C. Conclusions

The efficiency of an Archimedean-Type Hydrokinetic Turbine with fixed geometry has been investigated, varying the operative condition (i.e. the TSR) and the incidence angle. Comparing the performance curve of the Archimedean-Type Hydrokinetic Turbine with that of other hydrokinetic turbines (e.g. Savonious), they have the same operative range ($0 \leq TSR \leq 1.75$) and similar maximum performance (without Venturi devices, $C_p \sim 25 \div 35\%$).
The incidence angle has a paramount influence on the efficiency of the turbine, which can be reduced by a factor 4 (see Fig. 5). On the other hand, the influence of the incidence angle on the power production is smaller and, for certain angles, it is also favorable, increasing the performance (see Fig. 4). This states that a variation in the direction of a tidal stream lower than $50°$ has a minor effect on the power production, if this kind of turbine is used in a tidal energy system.

REFERENCES

[1] U. N. G. Assembly, "Resolutions and decisions adopted by the general assembly during its seventieth session: Volume i 70/1," 2015.
[2] T. O'Doherty, D. M. O'Doherty, and A. Mason-Jones, *Wave and Tidal Energy*, 1st ed. John Wiley & Sons Ltd., 2018, ch. Tidal Energy Technology, pp. 105–150.
[3] M. J. Khan, G. Bhuyan, M. T. Iqbal, and J. E. Quaicoe, "Hydrokinetic energy conversion systems and assessment of horizontal and vertical axis turbines for river and tidal applications: A technology status review," *Applied Energy*, vol. 86, no. 10, pp. 1823–1835, 2009.
[4] M. S. Guney, "Evaluation and measures to increase performance coefficient of hydrokinetic turbines," *Renewable and Sustainable Energy Reviews*, vol. 15, no. 8, pp. 3669–3675, 2011.
[5] N. D. Laws and B. P. Epps, "Hydrokinetic energy conversion: Technology, research, and outlook," *Renewable and Sustainable Energy Reviews*, vol. 57, pp. 1245–1259, 2016.
[6] G. Zitti, F. Fattore, A. Brunori, B. Brunori, and M. Brocchini, "Efficiency evaluation of an archimedean-type hydrokinetic turbine in a steady current," 13th International Conference on Hydrodynamics, Incheon, Korea on 2-6 September,, 2018.
[7] G. Zitti, F. Fattore, A. Brunori, B. Brunori, , and M. Brocchini, "Efficiency evaluation of a ductless archimedes turbine: laboratory experiments and numerical simulations," *Renewable Energy (Under Review)*, 2019.
[8] L. P. Chamorro, C. Hill, S. Morton, C. Ellis, R. E. A. Arndt, and F. Sotiropoulos, "On the interaction between a turbulent open channel flow and an axial-flow turbine," *Journal of Fluid Mechanics*, vol. 716, pp. 658–670, 2013.
[9] W. C. Schleicher, J. D. Riglin, and A. Oztekin, "Numerical characterization of a preliminary portable microhydrokinetic turbine rotor design," *Renewable Energy*, no. 76, pp. 234–241, 2015.
[10] K. Golecha, T. I. Eldho, and S. V. Prabhu, "Influence of the deflector plate on the performance of modified savonius water turbine," *Applied Energy*, vol. 88, no. 9, pp. 3207–3217, 2011.
[11] N. K. Sarma, A. Biswas, and R. D. Misra, "Experimental and computational evaluation of savonius hydrokinetic turbine for low velocity condition with comparison to savonius wind turbine at the same input power," *Energy conversion and management*, vol. 83, pp. 88–98, 2014.
[12] A. Kumar and R. Saini, "Performance parameters of savonius type hydrokinetic turbine–a review," *Renewable and Sustainable Energy Reviews*, vol. 64, pp. 289–310, 2016.
[13] D. Kumar and S. Sarkar, "A review on the technology, performance, design optimization, reliability, techno-economics and environmental impacts of hydrokinetic energy conversion systems," *Renewable and Sustainable Energy Reviews*, vol. 58, pp. 796–813, 2016.

[14] A. Kumar and R. P. Saini, "Performance analysis of a savonius hydrokinetic turbine having twisted blades," *Renewable Energy*, vol. 108, pp. 502–522, 2017.
[15] A. Betz, "The maximum of the theoretically possible exploitation of wind by means of a wind motor," *Wind Engineering*, vol. 37, no. 4, pp. 441–446, 2013.
[16] *ANSYS Fluent Tutorial Guide*. ANSYS, Inc. Release 18.0, (2017).
[17] F. R. Menter, "Two-equation eddy-viscosity turbulence models for engineering applications," *AIAA journal*, vol. 32, no. 8, pp. 1598–1605, 1994.
[18] B. Andersson, R. Andersson, L. Håkansson, M. Mortensen, R. Sudiyo, and B. Van Wachem, *Computational fluid dynamics for engineers*. Cambridge University Press, (2011).
[19] J. Riglin, F. Carter, N. Oblas, W. C. Schleicher, C. Daskiran, and A. Oztekin, "Experimental and numerical characterization of a full-scale portable hydrokinetic turbine prototype for river applications," *Renewable Energy*, vol. 99, pp. 772–783, 2016.
[20] M. J. Khan, M. T. Iqbal, and J. E. Quaicoe, "River current energy conversion systems: Progress, prospects and challenges," *Renewable and Sustainable Energy Reviews*, vol. 12, no. 8, pp. 2177–2193, 2008.
[21] M. Ragheb and A. Ragheb, *Wind Turbines Theory - The Betz Equation and Optimal Rotor Tip Speed Ratio. Fundamental and Advanced Topics in Wind Power*. InTech Open, 2011.